The Role of Convective Model Choice in Calculating the Climate Impact of Doubling CO_2

R. S. LINDZEN, A. Y. HOU AND B. F. FARRELL

Center for Earth and Planetary Physics, Harvard University, Cambridge, MA 02138

(Manuscript received 30 July 1981, in final form 26 February 1982)

ABSTRACT

The role of the parameterization of vertical convection in calculating the climate impact of doubling CO_2 is assessed using both one-dimensional radiative-convective vertical models and in the latitude-dependent Hadley-baroclinic model of Lindzen and Farrell (1980). Both the conventional 6.5 K km^{-1} and the moist-adiabat adjustments are compared with a physically-based, cumulus-type parameterization. The model with parameterized cumulus convection has much less sensitivity than the 6.5 K km^{-1} adjustment model at low latitudes, a result that can be to some extent imitated by the moist-adiabat adjustment model. However, when averaged over the globe, the use of the cumulus-type parameterization in a climate model reduces sensitivity only ~34% relative to models using 6.5 K km^{-1} convective adjustment. Interestingly, the use of the cumulus-type parameterization appears to eliminate the possibility of a runaway greenhouse.

1. Introduction

Recent studies have shown that the atmospheric carbon dioxide concentration has increased by ~15% in the past century (e.g., Keeling, *et al.*, 1976). The causes seem to be primarily the burning of fossil fuels and deforestation. If this trend continues, the amount could conceivably double by the early parts of the twenty-first century, as projected by Bacastow and Keeling (1973) and Hoffert (1974). Since CO_2 absorbs thermal radiation leaving the earth's surface, an increase of CO_2 content would lead to a warming of the troposphere; this in turn would cause an increase of water vapor content in the atmosphere, which has an even stronger positive feedback on temperature. As a result, it is expected that increases in the atmospheric CO_2 content will result in significant changes in the surface temperature.

The effect of an increase in CO_2 on the globally-averaged surface temperature has been estimated in a number of studies based on one-dimensional, "vertical-column energy-balance" radiative-convective models. [See Ramanathan and Coakley (1978) for an extensive review on the existing radiative-convective models.] Using the "lapse-rate adjustment" procedure developed by Manabe and Strickler (1964) to simulate the effects of moist convection in a radiative-convective model, Manabe and Wetherald (1967) estimated that increasing the CO_2 content from 300 to 600 ppm would raise the global surface temperature by 2.4 K. Later Manabe (1971) obtained a 1.95 K increase with an improved radiative model. Subsequent model studies, including simulations by general circulation models, have predicted increases between 2 to 4 K for a doubling of the present-day CO_2 amount (Manabe and Wetherald, 1975; Schneider, 1975; Ramanathan, *et al.*, 1979; Manabe and Wetherald, 1980). Most recently, Manabe and Stouffer (1979, 1980) reported a global-mean increase of 4 K for a quadrupling of the present-day CO_2 amount and showed that ice/snow feedbacks modestly increase the sensitivity. In view of the uncertainties involved in modeling the complex radiative and convective processes in the atmosphere, these estimates are not all that different.

The lapse-rate adjustment scheme is a numerical procedure by which the computed local lapse rate is set to a specified "critical lapse rate," whenever it becomes supercritical. This process is carried out for all supercritical layers without changing the mass or total energy of the column. This produces throughout the bulk of the troposphere a "convective regime" characterized by a constant lapse rate given by the critical lapse rate. Usually this critical value is taken to be 6.5 K km^{-1} for a standard atmosphere. Although in terms of its climatic impact a 2 K increase in the globally-averaged surface air temperature is a significant perturbation, it corresponds to only a 0.7% change of the global surface temperature of 288 K. A change of this size can result from a change of a mere 0.2 K km^{-1} in the tropospheric lapse rate. Clearly, the predicted increases are small responses in the context of model uncertainties. Recent studies show that the global-mean surface temperature sensitivity may be reduced by 25–60% using the moist-adiabatic lapse rate in an adjustment model (Hansen

0022-4928/82/061189-17$08.25

et al. 1981; Chylek and Kiehl, 1981; Ramanathan, 1981; Hummel and Kuhn, 1981a). In this study we re-examine this effect using a physically-based parameterization for convection rather than an adjustment. We show that the reasons for reduced sensitivity are as follows: 1) the heat lost from the surface through evaporation and upward sensible heat fluxes is deposited by cumulus clouds at a higher level where it is more effectively radiated to space; and 2) the freedom of a variable lapse rate allows radiative perturbations to be accommodated locally near the tropopause, without being carried through a fixed lapse rate to the surface. As a result, the perturbation response of a cumulus model tends to concentrate at the cloud-top levels rather than the uniform response of a fixed-lapse-rate model; this would then lead to a smaller greenhouse feedback. These features are indeed mimicked by moist-adiabatic adjustments for the present problem, but it is not clear that this will be generally true.

Our physically-based cumulus parameterization is that outlined by Lindzen (1979, 1981), which is a slight generalization of that given in Stevens and Lindzen (1978). These convective models are briefly described in Section 2. We attempt first to compare the various convective schemes in the context of a simple, self-consistent radiative model that responds directly to the solar forcing, namely, a non-grey model based on Rodger's (1967) emissivity formulations for water vapor and CO_2 absorptions and Lindzen and Will's (1973) approximation for ozone heating. We are able to show that the cumulus parameterization is indeed less sensitive to radiative perturbations than the convective adjustment for sufficiently high surface temperatures. Under tropical conditions the sensitivity to doubling CO_2 can be reduced by as much as 80% by using cumulus parameterization, while at high latitudes the two convective models are comparable. Averaging the radiative-convective results globally reveals a net reduction of 34% by the cumulus model in the global sensitivity to CO_2 doubling. These calculations are presented in Section 3. In Section 4 we study the effects of convective parameterization in the global climate model developed by Lindzen and Farrell (1980). Our results, consistent with GCM results (Manabe and Wetherald, 1975; Manabe and Stouffer. 1980), show that globally-averaged sensitivities are increased by ice/snow feedbacks, and that sensitivities at high latitudes are amplified compared to those in regions free of ice/snow. In this case too, however, sensitivities are decreased by $\sim$30% when convective adjustment is replaced by the cumulus-type parameterization. Section 4 shows that one-dimensional calculations are easily extended to a global latitude-dependent model.

2. Simple models of moist convection

a. The conventional lapse-rate adjustment

A widely used numerical procedure that simulates the effects of small-scale convection in one-dimensional, radiative-convective calculations is to set the local lapse rate to a specified "critical" lapse rate whenever it becomes supercritical; otherwise the condition of local radiative equilibrium is satisfied. The scheme effectively cools the surface and redistributes heat vertically, while requiring that the total "convective heating" induced by adjustment processes be equal to the net radiative deficit at the ground. The radiative-convective equilibrium temperature profile is balanced locally by radiative cooling and the "convective heating" implied by the adjustment of lapse rates. In a steady state, the net outgoing longwave radiation must equal the net incoming solar insolation. For what we shall call the "conventional lapse-rate adjustment approach," we will calculate the radiative-convective equilibrium temperature as the steady-state solution to an initial-value problem. At every step in the forward time marching we apply the lapse-rate adjustment, following the numerical procedure outlined in Manabe and Strickler (1964) and Manabe and Wetherald (1967). For the critical lapse rate we adopt their value of 6.5 K km^{-1}, which roughly corresponds to the mean tropospheric lapse rate of the standard atmosphere. The implied small-scale convective heating rate Q_c at a given time step can be defined as

$$Q_c = \rho C_p \frac{(T - T_R)}{\Delta t}, \tag{1}$$

where C_p is the heat capacity of dry air, ρ the density of air, T_R the instantaneous temperature profile determined by radiation alone, T is T_R with the supercritical lapse rates adjusted to the specified critical value, and Δt is the size of the time step. Since it is stipulated in the adjustment process that no temperature discontinuity should exist (hence the ground temperature equals the air temperature at the ground), and that there is no heat exchange at the ground, the vertical integral of Q_c must balance the radiative deficit at the surface.

b. Physical parameterization of convection

An alternative to the semi-empirical, lapse-rate adjustment approach is the physically-based cumulus parameterization described in Lindzen (1978, 1979, 1981) and Stevens and Lindzen (1978). This parameterization is generalized to include dry convection in Lindzen (1978). Here we will briefly summarize the procedures. The convective heating originates in the fluxes of latent and sensible heats from the surface. The surface fluxes are given by

$$E = C_D u_*[q_s(T_*) - q(T(0))], \quad (2a)$$

$$F_s = C_D u_* C_p[T_* - T(0)], \quad (2b)$$

where E is the evaporation, F_s the sensible heat flux, C_D the aerodynamic drag coefficient, u_* a "gustiness" factor, $T(0)$ the air temperature at the ground, and T_* the ground temperature. The water vapor mixing ratios q and q_s are obtained as follows: The saturation mixing ratio q_s is given by the Clausius-Clapeyron relation as

$$q_s(T) = q_1 \exp\left[q_2\left(\frac{1}{273} - \frac{1}{T}\right)\right], \quad (3a)$$

where

$$q_1 = 0.622 e_s/p, \quad q_2 = L/R_v,$$

e_s is the equilibrium water vapor partial pressure at $T = 273$ K; p the total pressure, L the latent heat of evaporation, and R_v the gas constant of air. We let r denote the relative humidity. Then

$$q(T) = rq_s(T). \quad (3b)$$

Following the interpretation given in Stevens and Lindzen (1978), we can express the convective heating rate as

$$Q_c = -\frac{dF_c}{dz} = C_p M_c\left(\frac{dT}{dz} + \frac{g}{C_p}\right), \quad (4)$$

where F_c denotes the convective heat flux, and the convective mass flux M_c, as a first approximation, is taken to be constant between $z = 0$ and the top of the convective region at $z = Z_T$. The detrainment level Z_T is given by the intersection of the surface moist enthalpy with the ambient dry enthalpy, i.e.,

$$C_p T(Z_T) + gZ_T = C_p T(0) + Lq(0), \quad (5)$$

where $q(0)$ denotes $q[T(0)]$. The value of M_c is chosen so that the integrated heating given by (4) equals the heat released from the surface; that is

$$C_p M_c \int_0^{Z_T}\left(\frac{dT}{dz} + \frac{g}{C_p}\right)dz = LE + F_s$$

$$= C_p M_c\left[T(Z_T) - T(0) + \frac{gZ_T}{C_p}\right] = M_c L q(0), \quad (6)$$

or

$$M_c = \frac{LE + F_s}{Lq(0)}$$

$$= \frac{C_D u_*\{L[q_s(T_*) - q(0)] + C_p[T_* - T(0)]\}}{Lq(0)}. \quad (7)$$

Here M_c has the property of becoming infinite as $L \to 0$. In the light of (4), this means that the parameterization reverts to the dry convective adjustment in this case. Since in thermal equilibrium the temperature must be continuous at the cloud top, where Q_c vanishes, the lapse rate immediately below Z_T must be adiabatic, corresponding to neutral static stability. Above the cloud top, $Q_c = 0$, and the stratosphere is in local radiative equilibrium. Incorporating this parameterized heating into a radiative model, we can obtain the radiative-convective equilibrium temperature with both the convective heating rate and the actual lapse rate profile calculated explicitly. We will refer to this as the "cumulus" radiative-convective model.

It should be noted that (7) relates cumulus mass flux to surface fluxes. In fact, dependence on low-level convergence should also be included (Lindzen, 1981). However, in the context of our global calculations presented in Section 4 this is unimportant. The point is that the details of cumulus parameterization are only important in the Hadley regime, where Schneider (1977) has shown that the response is primarily to total heating and where the effects of low-level convergence and divergence cancel (*viz.*, Section 4).

3. Results for radiative-convective equilibrium

a. Case studies

The state of radiative-convective equilibrium is obtained as the steady-state solution to an initial-value problem. The radiative model, which is based on Rodgers' (1967) emissivity approximation for the longwave H_2O and CO_2 absorptions and Lindzen and Wills' (1973) formulation for the shortwave ozone heating, is described in the Appendix. The effect of clouds on the earth's climate sensitivity is still poorly understood. The inclusion of fixed clouds would introduce a number of parameters such as cloud height, thickness, coverage and radiative properties. Since it is not clear whether a fixed-cloud model based on parameters derived from uncertain and highly variable data can predict the climate sensitivity of an atmosphere with interactive clouds, we have decided to use a clear-sky radiative model to test the role of convective models. Also, Hummel and Kuhn (1981b) have recently shown that major sensitivity differences exist between fixed and interactive cloud models in one-dimensional radiative-convective calculations. Obviously, our ignorance concerning clouds is, as has often been noted, a serious source of uncertainty in sensitivity studies. The solution to this problem is less obvious.

The finite-difference model has a vertical resolution of 40 levels between $z = 0$ and 40 km. Steady-state solutions correspond to net heating rates $<10^{-5}$ K day^{-1} at all levels. For calculations presented here we have adopted the following parametric values: the

constants for the saturation mixing ratio of water vapor in (3) are taken to be $q_1 = 3.751 \times 10^{-3}$ at $p = 1000$ mb and $q_2 = 5.417 \times 10^3$ K^{-1}. The relative humidity profile is taken from Manabe and Wetherald (1967) with the surface relative humidity set at 80%. The value used for the drag formula parameter $C_D u_*$ in (2), which controls evaporation and sensible heat fluxes at the surface, unless otherwise specified, is assumed to be 0.0124 m s^{-1}. If we interpret C_D as the aerodynamic drag coefficient over a smooth ocean surface [Priestly (1959) gives $C_D = 0.0024$], then the value $C_D u_* = 0.0124$ m s^{-1} corresponds to a surface boundary layer velocity of 5 m s^{-1}. Alternatively, we can model surface evaporation and sensible heat fluxes in terms of small-scale turbulent mixing, as in Sarachik (1978): that is, $C_D u_*$ can be replaced by $C'_D u'_*$, where u'_* is a characteristic turbulent mixing velocity; C'_D is the turbulent mixing coefficient defined as $\kappa/\ln(L_m/L_R)$; L_R is the roughness parameter for a smooth surface $\sim$0.1 m, L_m the Monin-Obukhov length $\sim$10 m, and κ the von Kármán constant = 0.4, or $C'_D = 0.124$. In this case, the reference value $C'_D u'_* = 0.0124$ m s^{-1} corresponds to $u'_* = 0.1$ m s^{-1}.

Since in these calculations the amount of ozone heating is specified, we will regard the solar radiation absorbed at the ground ($F_{\odot *}$) as an independent parameter. $F_\odot$, the solar radiation the system actually receives, is taken to be the net outgoing longwave flux at the top of the model atmosphere in radiative-convective equilibrium. It should be noted that for a given radiative-convective temperature profile characterized by the surface temperature T_*, $F_\odot$ represents a unique outgoing infrared flux at the model top. Extensive use will be made of this interpretation in Section 4. For easy reference $F_\odot$ can be expressed in terms of the observed solar flux distribution of the form given in Lindzen and Farrell (1980), i.e.,

$$F_\odot(\theta, \alpha) = \tfrac{1}{4}(1 - \alpha)S_\odot[1 - 0.482P_2(\sin\theta)], \quad (8)$$

where θ is latitude, α albedo, P_2 the second Legendre polynomial, and the solar constant $S_\odot$ is taken to be 1380 W m^{-2}.

Numerical solutions for radiative-convective equilibrium profiles were calculated for a series of values of solar flux $F_\odot$ ranging from 420 to 30 W m^{-2}. To test the models' sensitivities to CO_2 perturbations, for each value of $F_\odot$ results were obtained for the standard and doubled amounts of CO_2 using the 6.5 K km^{-1} lapse-rate adjustment model, the moist-adiabatic adjustment model, and the cumulus model. In the following section we will compare in detail the model results for two cases: (i) $F_\odot = 274$ W m^{-2}, a value for which the lapse-rate adjustment model gives the reference surface temperature $T_* = 288$ K, close to the global-mean surface temperature calculated by Manabe and Wetherald (1967) and later obtained by Manabe (1971) using an improved radiation model. This solar flux value is slightly higher than a typical incident solar flux value at midlatitudes given an albedo of 0.3. The second case (ii) is $F_\odot = 353$ W m^{-2}, which corresponds to $\alpha = 0.18$ at the equator according to (8). These results are summarized in Tables 1 and 2.

Table 1 gives the radiative-convective equilibrium results for the case $F_\odot = 274$ W m^{-2}. The notations used here are T_* is the ground temperature; $T(0)$ the air temperature at the ground ($z = 0$); $\Delta_* = T_* - T(0)$ is the temperature discontinuity at the ground; ΔT_* and $\Delta T(0)$ are the increases in T_* and $T(0)$, respectively, due to a doubling in CO_2 content; $\bar{T}$ is the mass-weighted vertical average of $T(z)$; $\Delta\bar{T}$ is the change in $\bar{T}$ resulting from doubling the CO_2 amount; Z_T is the height of the convective region referred to as the "cloud top;" $F_{\odot *}$ is the solar flux absorbed at the ground; $\langle Q_c \rangle$ is the total (vertically integrated) convective heating; in cases that the surface flux condition is $\Delta_* \equiv 0$ this is given by the radiative deficit at the surface; with the parameterized surface-flux condition this equals the total convective flux $LE + F_s$; P is the precipitation inferred from LE; and $q[T(0)]$ is the water vapor mixing ratio defined in (3b). The Bowen ratio is by definition the quotient of the surface sensible heat flux and the latent heat release at the surface, i.e., F_s/LE.

For values of u'_* ranging from 0.15 to 0.05 m s^{-1}, Table 1 shows that the surface temperatures given by the various models differ by less than 1% for the "midlatitude" value of $F_\odot = 274$ W m^{-2}. In the conventional 6.5 K km^{-1} lapse-rate adjustment model, the surface flux boundary condition $\Delta_* = 0$ requires $T_* = T(0)$. A doubling of CO_2 leads to an increase of 1.978 K in the surface temperature, similar to that reported by Manabe (1971). In the case of the cumulus model, the parameterized surface energy flux ($LE + F_s$) allows a temperature discontinuity at the ground. The results show that the effect of the surface drag coefficient $C'_D u'_*$ is to regulate the size of Δ_* by controlling the rate of evaporation and sensible heat fluxes without significantly altering the ground temperature itself. Ultimately, as $C'_D u'_* \to 0$, the solution would, of course, approach the pure radiative equilibrium state. In cases where the small-scale turbulent mixing in the surface layer is sufficiently vigorous to maintain a temperature discontinuity of the order of only a couple of degrees at the surface, the cumulus model is indeed less sensitive to CO_2 perturbations than the adjustment model, as argued in Section 1. A similar sensitivity reduction is also obtained in the case of the moist-adiabat adjustment model with the parameterized fluxes at the surface. This is in agreement with the 25–60% reduction found by Hummel and Kuhn (1981a) using a considerably more elaborate radiation model. It will become evident as we later examine the vertical structures of these solutions that the adjustment to

TABLE 1. Radiative-convective equilibrium results for $F_\odot = 274$ W m^{-2}.

Surface flux condition	6.5 K km^{-1} adjustment model				Moist-adiabat adjustment model		Cumulus model					
	$F^\uparrow(z=0) = \sigma T_*^4 = \sigma T(0)^4$		$F^\uparrow(z=0) = \sigma T_*^4 = F_{\odot *} + F^\downarrow(z=0) - (LE + F_s)$									
			$u'_* = 0.10$ m s^{-1}		$u'_* = 0.10$ m s^{-1}		$u'_* = 0.15$ m s^{-1}		$u'_* = 0.10$ m s^{-1}		$u'_* = 0.05$ m s^{-1}	
	Standard CO_2	Double CO_2	Standard CO_2	Double CO_2	Standard CO_2	Double CO_2	Standard CO_2	Double CO_2	Standard CO_2	Double CO_2	Standard CO_2	Double CO_2
T_* (K)	288.003	289.981	288.809	290.742	288.571	290.082	289.129	290.574	289.751	291.212	290.536	292.524
$T(0)$ (K)	288.003	289.981	286.286	288.526	285.801	287.512	288.035	289.631	287.348	288.986	284.841	287.173
Δ_* (K)	0	0	2.523	2.216	2.770	2.57	1.094	0.943	2.403	2.226	5.695	5.351
ΔT_* (K)	—	1.978	—	1.933	—	1.511	—	1.445	—	1.461	—	1.988
$\Delta T(0)$ (K)	—	—	—	1.978	—	1.711	—	1.596	—	2.240	—	2.322
$\bar{T}$ (K)	246.346	247.571	244.935	246.427	243.910	246.048	243.015	244.829	241.968	243.783	238.553	240.997
$\Delta\bar{T}$ (K)	—	1.225	—	1.492	—	2.138	—	1.814	—	1.815	—	2.444
Z_T (km)	13.93	14.50	13.79	14.07	10.57	10.63	9.51	9.85	9.40	9.67	9.02	9.32
$F_{\odot *}$ (W m^{-2})	265.5	265.5	265.5	265.5	265.5	265.5	265.5	265.5	265.5	265.5	265.5	265.5
$\langle Q_c \rangle$ (W m^{-2})	157.052	160.605	142.506	147.462	147.658	153.008	155.194	160.980	145.747	151.333	122.020	128.203
P (cm year^{-1})	—	—	129.069	143.231	129.638	142.055	166.207	178.089	136.417	148.136	91.121	105.118
$q(0)$ (g kg^{-1})	8.44	9.59	7.54	8.73	7.30	8.17	8.45	9.38	8.08	8.99	6.85	7.99
Bowen ratio	—	—	0.282	0.230	0.304	0.264	0.151	0.123	0.258	0.224	0.408	0.350

TABLE 2. Radiative-convective equilibrium results for $F_\odot = 353$ W m^{-2}.

Surface flux condition	6.5 K km^{-1} adjustment model		Moist-adiabat adjustment model		Cumulus model	
	$F^\uparrow(z=0) = \sigma T_*^4 = \sigma T(0)^4$		$F^\uparrow(z=0) = \sigma T_*^4 = F_{\odot *} + F^\uparrow(z=0) - (LE + F_s)$			
			$u'_* = 0.10$ m s^{-1}		$u'_* = 0.10$ m s^{-1}	
	Standard CO_2	Double CO_2	Standard CO_2	Double CO_2	Standard CO_2	Double CO_2
T_* (K)	321.886	326.425	309.075	310.260	308.876	309.692
$T(0)$ (K)	321.886	326.425	308.118	309.469	307.626	308.522
Δ_* (K)	0	0	0.957	0.791	1.250	1.170
ΔT_* (K)	—	4.539	—	1.185	—	0.816
$\Delta T(0)$ (K)	—	4.539	—	1.351	—	0.896
$\bar{T}$ (K)	273.986	277.393	278.292	280.123	276.102	277.650
$\Delta\bar{T}$ (K)	—	3.407	—	1.831	—	1.548
Z_T (km)	17.14	17.57	18.50	19.20	15.20	15.71
$F_{\odot *}$ (W m^{-2})	345	345	345	345	345	345
$\langle Q_c \rangle$ (W m^{-2})	330.363	360.073	298.146	306.486	313.358	321.931
P (cm year^{-1})	—	—	360.482	373.813	374.727	387.009
$q(0)$ (g kg^{-1})	61.09	77.20	28.80	31.10	28.00	29.47
Bowen ratio	—	—	0.0415	0.0331	0.052	0.047

the local moist-adiabatic lapse rate succeeds in mimicking the main features of the cumulus model which lead to reduced sensitivities.

In order to demonstrate that the reduced sensitivities in the cumulus and the moist-adiabat adjustment model results cannot be accounted for in terms of the different surface flux conditions, we performed a calculation using the 6.5 K km^{-1} adjustment model with the $T_* \equiv T(0)$ condition replaced by the parameterized flux condition at the lower boundary. The results are shown in the second column of Table 1. In this case ($u'_* = 0.1$ m s^{-1}), the model develops a temperature discontinuity $\Delta_* = 2.52$ K for standard CO_2, the sensitivity $\Delta T(0)$ increases by 13% from that for the $\Delta_* \equiv 0$ model, while ΔT_* remains virtually unaffected. Hence, the sensitivity differences shown by the cumulus and the moist-adiabat adjustment models are, in fact, consequences of the convection models rather than the different surface flux conditions.

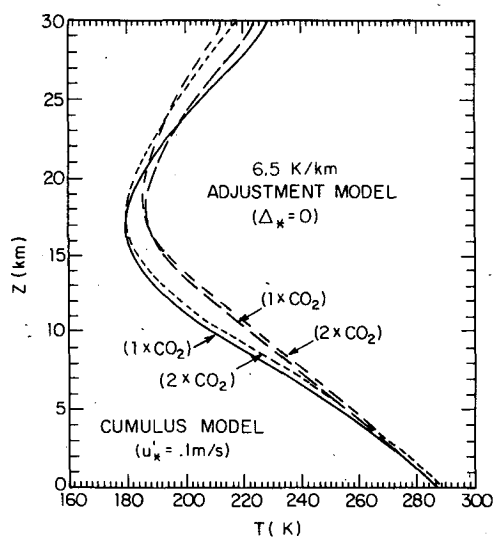

FIG. 1. Radiative convective equilibrium temperatures for $F_\odot = 274$ W m^{-2}.

Based on Table 1 we conclude that at midlatitudes the response of a cumulus model with $\Delta_* \leqslant 2.4$ K is at least 26% less sensitive than the 6.5 K km^{-1} adjustment model when the current CO_2 content is doubled, and that the moist-adiabat adjustment model to some extent behaves like the cumulus model.

Figs. 1–6 display the vertical structures of the various quantities. The 6.5 K km^{-1} adjustment results shown in these figures are for the $\Delta_* \equiv 0$ case, the counterpart of that of Manabe and Wetherald (1967) or Manabe (1971). Fig. 1 compares the radiative-convective equilibrium profiles of the 6.5 K km^{-1} adjustment model and the cumulus model. (The moist-adiabat adjustment profile, which lies close to the cumulus profile between the 6.5 K km^{-1} and cumulus curves, is omitted.) The temperature profiles of the constant lapse-rate adjustment model show a uniform lapse rate of 6.5 K km^{-1} over most of the convective region below $Z_T = 14$ km. The "cloud tops" in the cumulus model are located at the comparatively lower heights around 9.5 km (see Table 1), closer to the observed midlatitude value of 11 km (Minzner, 1977).

In Fig. 2 we see that the tropospheric lapse rates produced by the cumulus model are more realistic than a constant lapse rate of 6.5 K km^{-1}, the general shape follows the moist adiabat in the lower troposphere and approaches the dry adiabatic value near the "cloud top". Over the bulk of the troposphere,

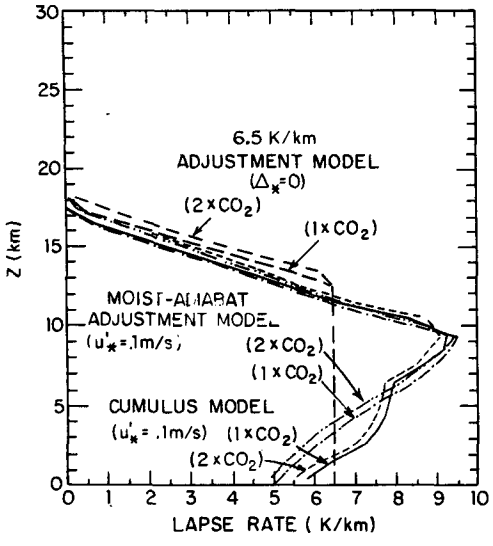

FIG. 2. Lapse rates for $F_\odot = 274$ W m^{-2}.

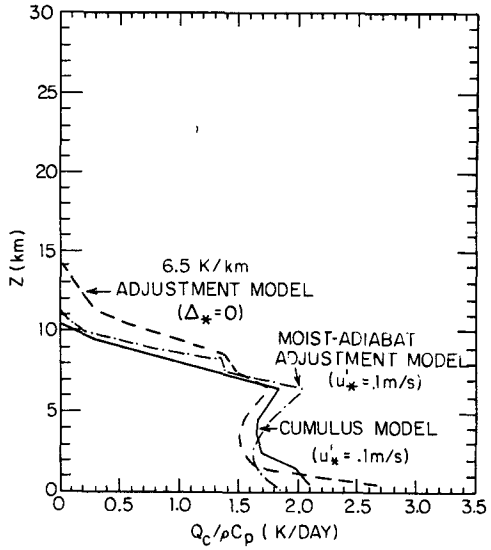

FIG. 4. Convective heating rates in the standard CO_2 case for $F_\odot = 274$ W m^{-2}.

these moist adiabatic lapse-rate profiles are in general agreement with the observational data of Oort and Rasmusson (1971), as plotted in Fig. 3 of Ramanathan and Coakley (1978). The $\Delta T(z)$ resulting from doubled CO_2 amount is shown in Fig. 3. The constant lapse rate of the 6.5 K km^{-1} adjustment model results in a uniform perturbation of temperature through the convective region as can be seen in Fig. 1. In contrast to this uniform response, maximum temperature changes in both the cumulus model and the moist-adiabat adjustment model are aloft near the "cloud tops". This suggests that these variable lapse-rate models, when perturbed, can radiate to space more efficiently than the fixed lapse-rate adjustment model, and at the same time produce less greenhouse feedback. These effects can be expected to be more pronounced at larger solar-flux values where the cloud-top level will be higher. The convective heating rates in Fig. 4 show that the various convection schemes lead to more or less similar heating profiles, the main difference being that the 6.5 K km^{-1} adjustment model tends to produce large heating rates near the surface relative to those in the interior, while both the cumulus and the moist-adiabat adjustment model are more effective in depositing heat higher in the troposphere. Fig. 5 shows radiative heating rates due to the various absorbers balancing the convective heating rates for the 6.5 K

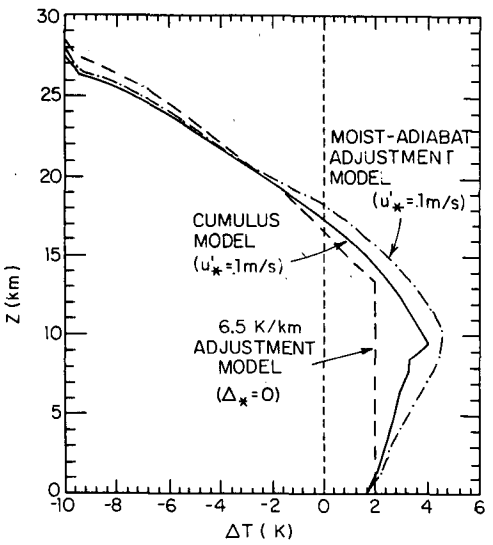

FIG. 3. Temperature changes resulting from doubling the current CO_2 content for the $F_\odot = 274$ W m^{-2} case.

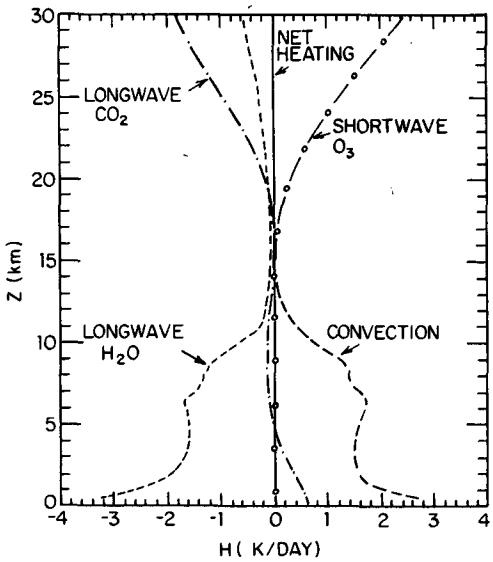

FIG. 5. Heating rates of the 6.5 K km^{-1} adjustment model in the standard CO_2 case for $F_\odot = 274$ W m^{-2}.

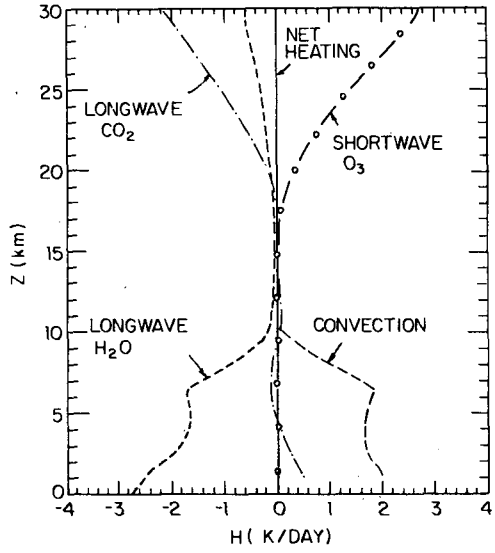

FIG. 6. Heating rates of the cumulus model in the standard CO_2 case for $F_\odot$ = 274 W m^{-2}.

km^{-1} adjustment model. Fig. 6 shows the same balance for the cumulus model. Results of this simple non-grey radiation model compare well with the heating profiles given by the more detailed emissivity model of Manabe and Strickler (1964). Not surprisingly, the main difference is the slight CO_2 warming in the lower troposphere in the present model since the current CO_2 formulation takes into account the effect of the overlap of water vapor in the 15 μ region.

Radiative-convective equilibrium results for the case $F_\odot$ = 353 W m^{-2} are summarized in Table 2. Compared with the "midlatitude" results given in Table 1, both the surface temperature and the cloud-top level are higher, and moist convection plays a more prominant role in determining the tropospheric temperature. We would then expect that the "negative-feedback" mechanisms in the cumulus and moist-adiabat adjustment models to operate more effectively, thereby producing a more pronounced reduction in sensitivities. Indeed, we see that for a doubling of CO_2 the ΔT_* for the cumulus model is 82% less than for the 6.5 K km^{-1} adjustment model, and the moist-adiabat adjustment model shows a similar reduction of 74%. To some extent these differences are attributable to the fact that the 6.5 K km^{-1} adjustment model maintains a higher surface temperature than the 309 K given by the other two models. However, as our latitudinal calculations will show in Section 2b, the sensitivity of the 6.5 K km^{-1} model at T_* = 309 K is still roughly twice that of the cumulus model at the same surface temperature (see Figs. 11 and 13). Fig. 7a shows that changes in convective heating rates in the 6.5 K km^{-1} adjustment model are more or less uniform throughout the troposphere; in particular, the perturbation heating is significant at low levels, while in the cumulus model these changes are confined mainly to the cloud-top region. Fig. 7b shows that the adjustment to local moist-adiabatic lapse rates achieves a qualitatively similar perturbation heating response as the cumulus model. The corresponding temperature changes are plotted in Fig. 8. The 6.5 K km^{-1} adjustment model shows a constant ΔT over the bulk of the convective region, while in the other two models responses are concentrated in the cloud-top regions. This clearly shows that an important difference between a variable-lapse-rate model and a

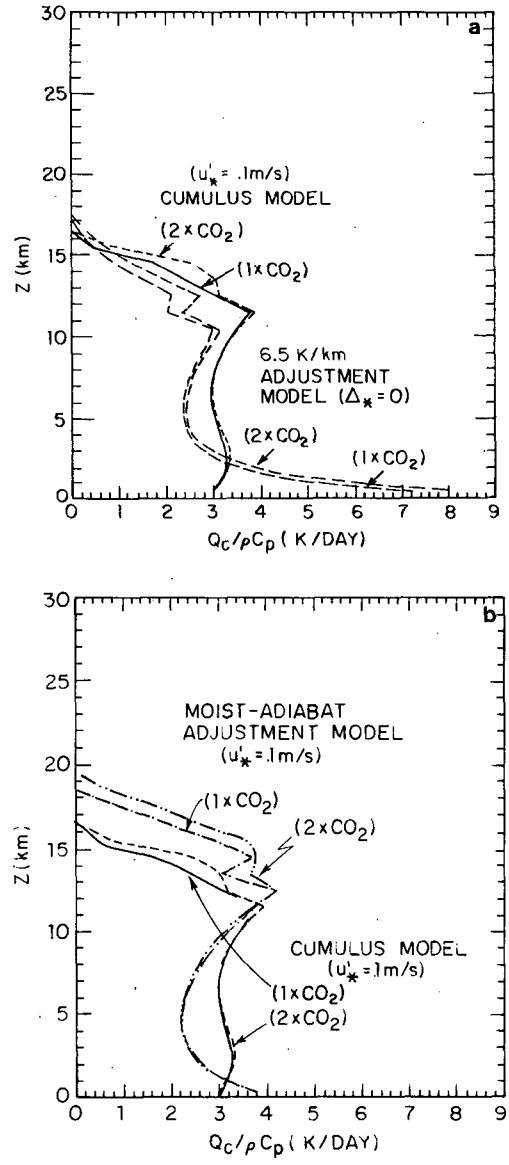

FIG. 7. Convective heating rates for (a) the 6.5 K km^{-1} adjustment model and the cumulus model for the $F_\odot$ = 353 W m^{-2} case and (b) for the moist-adiabat adjustment model and the cumulus model for the $F_\odot$ = 353 W m^{-2} case.

fixed-lapse-rate model is that the former permits local adjustments to radiative perturbations at levels where it can radiate efficiently to space. Although the physical mechanism that makes this possible in the tropics is cumulus convection, adjusting the temperature profile to the local moist-adiabatic lapse rate can to some extent reproduce the cumulus model results. In the case of the 6.5 K km^{-1} adjustment model, the tropospheric lapse rate is effectively fixed, and radiative perturbations are distributed throughout the entire convective region since the rigid thermal profile must shift as a whole. This leads to temperature changes in the lower troposphere, which, in turn, produce significant greenhouse feedback. It is, therefore, not surprising that the 6.5 K km^{-1} adjustment model should show greater sensitivity than the cumulus model. The lapse rates are shown in Fig. 9a and 9b. The temperature profiles are shown in Figs. 10a and 10b. In Tables 1 and 2 we see that as $F_\odot$ increases from 274 to 353 W m^{-2}, the surface temperature rises by 6.6% in the cumulus model and 7.1% in the moist-adiabatic adjustment model, both values are significantly less than the 11.8% for the 6.5 K km^{-1} adjustment model; clearly, the latter is also more sensitive to perturbations in solar flux.

From these results we conclude that both the cumulus model and the moist-adiabat adjustment model are significantly less sensitive to perturbations in either the CO_2 content or the solar flux than the conventional 6.5 K km^{-1} adjustment model in the tropics. However, at high latitudes where convective heatings are comparatively small, these models are not noticeably different (see Figs. 11 and 14). Since for the cases treated here the surface temperatures given by the moist-adiabat adjustment model are not appreciably different from those of the cumulus model, in the following sections we will restrict consideration to only the cumulus model and the 6.5 K km^{-1} adjustment model.

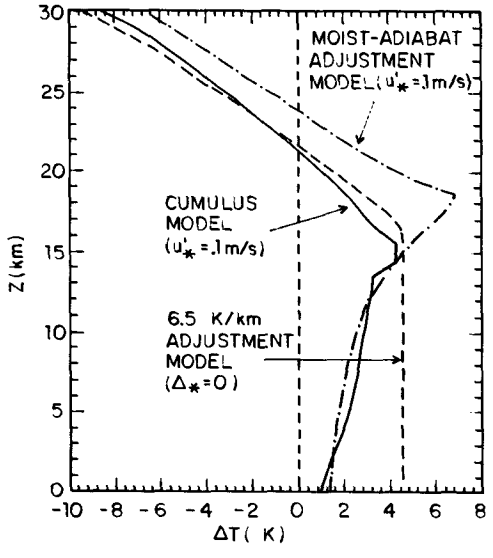

FIG. 8. Temperature changes resulting from doubling the current CO_2 content for the $F_\odot$ = 353 W m^{-2} case.

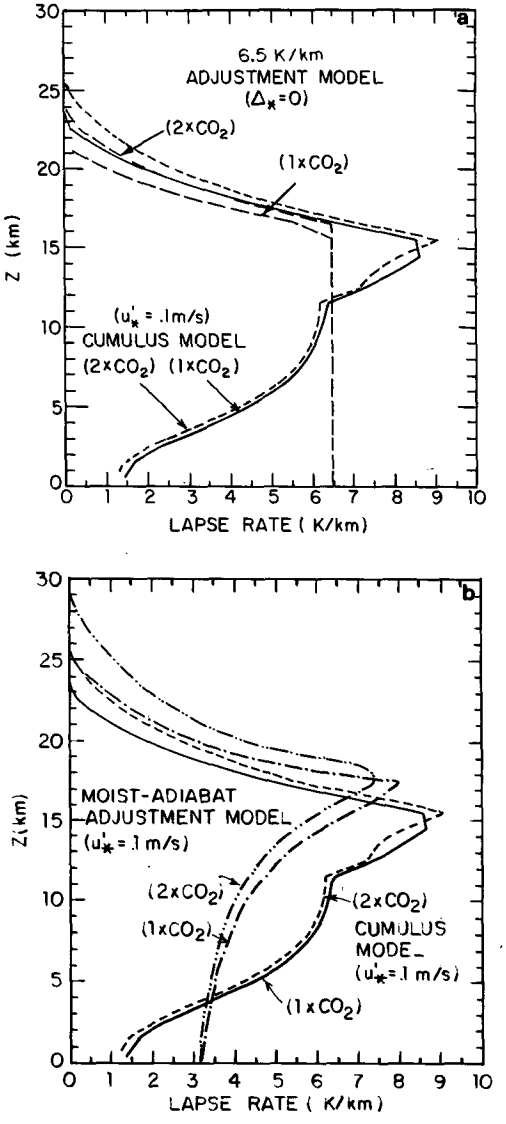

FIG. 9. Lapse rates of (a) the 6.5 K km^{-1} adjustment model and the cumulus model for $F_\odot$ = 353 W m^{-2} and (b) of the moist-adiabat adjustment model and the cumulus model for $F_\odot$ = 353 W m^{-2}.

b. *Radiative-convective equilibrium solutions as a function of the solar flux*

A series of radiative-convective equilibrium calculations were performed with the solar flux as an external parameter for both the standard and doubled amounts of CO_2. Fig. 11 shows the surface temperature as a function of $F_\odot$ for the standard CO_2 content. The curves are sixth-order polynomials fitted to the calculated temperatures. The figure clearly

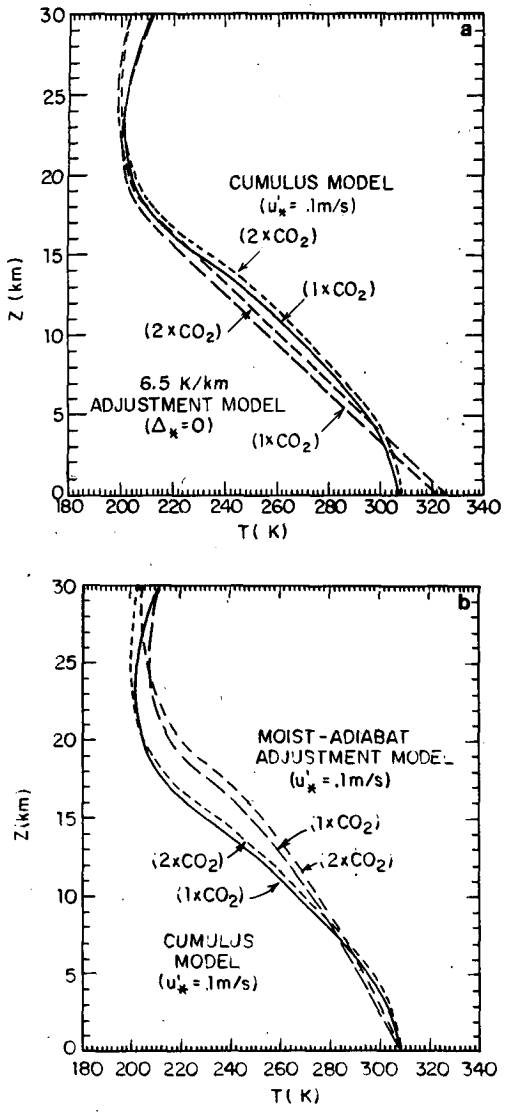

FIG. 10. Radiative-convective equilibrium temperatures of (a) the 6.5 K/km adjustment model and the cumulus model for $F_\odot$ = 353 W m^{-2} and (b) the moist-adiabat adjustment model and the cumulus model for $F_\odot$ = 353 W m^{-2}.

demonstrates the diminishing response of the cumulus model at large values of $F_\odot$, where the two models exhibit qualitatively different behaviors. As $F_\odot$ increases, the greenhouse feedback becomes more effective; ultimately, the adjustment model is unstable beyond $F_\odot \approx 368$ W m^{-2}. The cumulus model, on the other hand, responds by raising the temperature near the cloud-top level, thereby producing smaller greenhouse feedback. This results in the asymptotic behavior of the surface temperature shown in the figure, which suggests the real atmosphere may be much more stable to the greenhouse feedback than the fixed 6.5 K km^{-1} adjustment model might lead one to suspect. According to Fig. 11, once the surface temperature reaches a certain value (~315 K in the present case), the atmosphere becomes rather insensitive to further increase in the solar flux. This suggests that the earth's atmosphere, where water is the radiatively important constituent, will be unresponsive to the runaway greenhouse effect [see Ingersoll (1969) and Rasool and DeBergh (1970) for a discussion of this effect]. This figure also compares the model results with the observed outgoing infrared emission as a function of the surface temperature. The data are from Raschke *et al.* (1973) and Oort and Rasmusson (1971), as given in Held and Suarez (1974). The general agreement is apparent. The slight shift suggests that these models seem to require ~25 W m^{-2} more in solar flux in order to maintain the same temperature. This is probably a measure of the error due to the neglect of clouds in the IR budget. The only significant discrepancies are the two data points for 15° latitude, where the surface temperature is evidently insensitive to variations in solar fluxes, bearing some qualitative similarity to the cumulus model results. Radiative-convective equilibrium temperature profiles are plotted for several values of $F_\odot$ in Fig. 12. Note that as the solar flux increases, the tropospheric temperature of the 6.5 K km^{-1} adjustment model increases uniformly at all levels, while the temperature of the cumulus model rises more rapidly in the upper troposphere than at the surface. Here we see that for $T_* \approx 300$ K, roughly the equatorial surface temperature in our climate model results presented in Section 4, the radiative-convective equilibrium profile given by the cumulus model agrees well with the annual-mean values taken from Oort and Rasmusson (1971).

Fig. 13 shows ΔT_* as a function of the incoming

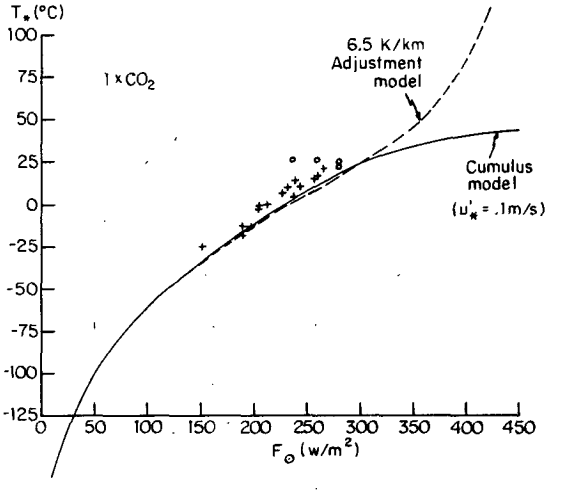

FIG. 11. Comparison of model results with data. The data points are taken from Fig. 8 of Held and Suarez (1974) [based on data from Raschke *et al.* (1973) and Oort and Rasmusson (1971)]. The circles are the four seasonal means for 15°N. The crosses are seasonal means for 30, 45 and 75°N.

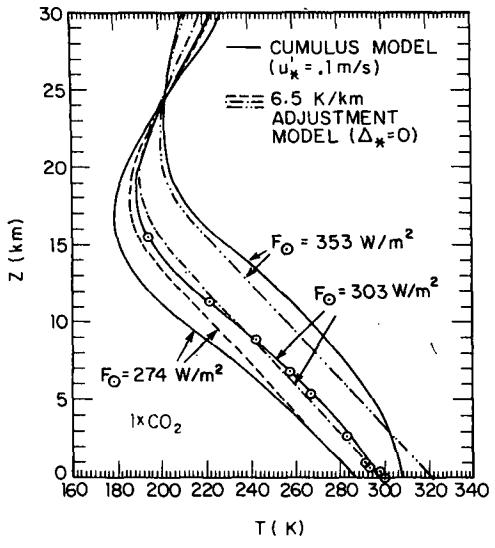

FIG. 12. Radiative-convective equilibrium temperature profiles for $F_\odot = 274$ W m^{-2}, $F_\odot = 303$ W m^{-2} and $F_\odot = 353$ W m^{-2}. The circles correspond to observed annual-mean values at the equator (Oort and Rasmusson, 1971).

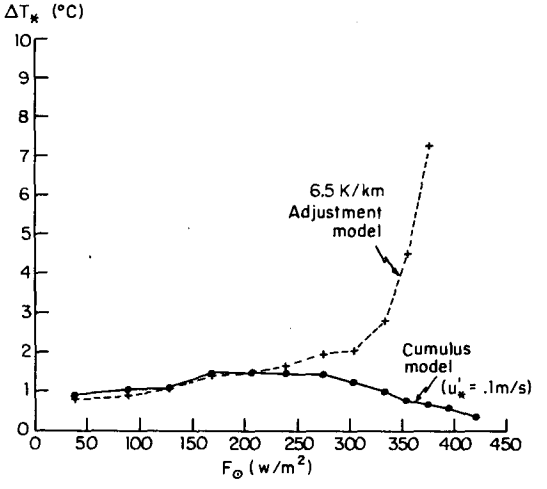

FIG. 13. Changes in surface temperature resulting from doubling the current CO_2 concentration as functions of the solar flux.

solar flux at the top of the model atmosphere. The reduced sensitivities of the cumulus model and the "runaway" response of the adjustment model at larger values of $F_\odot$ can be readily discerned. As expected, the influence of convection is small at high latitudes and results given by the two models are in close agreement. If we adopt the solar absorption distribution given by Hartmann and Short (1979) and ignore the ice albedo feedback,

$$(1 - \alpha) = 0.697 - 0.175P_2(\sin\theta), \qquad (9)$$

where P_2 is the second Legendre polynomial; substituting this into (8) gives $F_\odot = 335.88$ W m^{-2} at the equator and 93.3 W m^{-2} at the pole. Fig. 11 shows that these values fall just short of the region in which the two convection models are significantly different. From the range of solar flux values given in Fig. 13, we see that sensitivities of the two models are comparable until $F_\odot \gtrsim 240$ W m^{-2}, which corresponds to latitudes $\lesssim 36°$.

Despite obvious shortcomings, the most trivial way to estimate global sensitivity to doubling CO_2 is simply to average one-dimensional radiative-convective equilibrium results over all latitudes—ignoring transport and ice-albedo feedback. For reference purposes we will make such an estimate, and later compare it to climate model results. With the solar flux profile given by (8) and (9), we compute the global-mean T_* by integrating the approximate polynomial regression formula for the surface temperature as a function of the solar flux (see Fig. 11); the result is

$$T_*[°\text{C}] = \sum_0^6 C_i F_\odot^i \ [\text{W m}^{-2}], \qquad (10)$$

where the coefficients C_i ($i = 0, 6$) are given in Table 3. The resulting global-mean surface temperatures are 276.453 K for the standard CO_2 and an increase of 1.923 K for doubling the CO_2 content for the 6.5 K km^{-1} adjustment model. The corresponding figures for the cumulus model are 275.862 and 1.266 K. Thus, the cumulus model is ~34% less sensitive than the adjustment model.

TABLE 3. Polynomial regression coefficients for T_* ($F_\odot$).

	6.5 K km^{-1} adjustment model		Cumulus model	
	Standard CO_2	Double CO_2	Standard CO_2	Double CO_2
C_0	-1.8234×10^{2}	-1.8039×10^{2}	-1.8153×10^{2}	-1.8120×10^{2}
C_1	2.3430	2.2801	2.3520	2.3801
C_2	-1.8473×10^{-2}	-1.7240×10^{-2}	-1.8597×10^{-2}	-1.9069×10^{-2}
C_3	9.4912×10^{-5}	8.3668×10^{-5}	9.5361×10^{-5}	9.9308×10^{-5}
C_4	-2.6406×10^{-7}	-2.0932×10^{-7}	-2.6546×10^{-7}	-2.8115×10^{-7}
C_5	3.5202×10^{-10}	2.1695×10^{-10}	3.6942×10^{-10}	3.9826×10^{-10}
C_6	-1.5435×10^{-13}	-2.2028×10^{-14}	-2.0320×10^{-13}	-2.2315×10^{-13}

TABLE 4. Polynomial regression coefficients for $F_\odot(T_*)$.

	6.5 K km^{-1} adjustment model		Cumulus model	
	Standard CO_2	Double CO_2	Standard CO_2	Double CO_2
C'_0	2.3553×10^{2}	2.3120×10^{2}	2.2910×10^{2}	2.2529×10^{2}
C'_1	2.6594	2.6153	2.6153	2.6068
C'_2	2.3880×10^{-4}	1.9240×10^{-4}	3.7844×10^{-3}	3.7332×10^{-3}
C'_3	-1.2366×10^{-4}	-1.2593×10^{-4}	-9.0546×10^{-5}	-1.4378×10^{-4}
C'_4	-6.2447×10^{-8}	-8.0003×10^{-8}	6.1388×10^{-6}	5.5908×10^{-6}
C'_5	3.6250×10^{-9}	3.7039×10^{-9}	2.2682×10^{-7}	2.4476×10^{-7}
C'_6	0	0	2.5458×10^{-9}	2.8779×10^{-9}
C'_7	0	0	9.3330×10^{-12}	1.0809×10^{-11}

4. Climate sensitivity in a global model

As already noted, estimating the globally-averaged climate impact of doubling CO_2 by averaging local radiative-convective equilibria over all latitudes suffers from two important defects:

i) Transport mechanisms leave global-mean surface temperatures unchanged only if F, the outgoing infrared flux, is linear in surface temperature. Fig. 11 shows that this flux [which in radiative-convective equilibrium equals $(1 - \alpha)$ times the incident solar radiation] is not linear—although the deviation from linearity is not very great over the range of temperatures actually found in the atmosphere. However, the range of radiative-convective equilibrium temperatures is much larger.

ii) Radiative-convective equilibria do not readily allow the incorporation of ice-albedo feedback. Since the ice line is determined by surface temperature (generally ice is taken to occur when $T_* \leq -10°C$), one cannot totally use unrealistic equilibrium temperatures. This is a substantially more serious drawback.

Both these deficiencies are eliminated by means of the Hadley-baroclinic climate model of Lindzen and Farrell (1980). In this model radiative-convective equilibrium temperatures are modified by physically-determined Hadley and baroclinic horizontal heat transports to give realistic latitudinal distributions of temperature. Once one has realistic temperature distributions one can then include ice feedbacks.

The Lindzen-Farrell model incorporates two effects associated with the presence of ice and/or snow: i) increased albedo and ii) increased static stability near the surface. In Lindzen and Farrell the latter effect was incorporated by assuming that between $z = 0$ and $z = 0.25\ H$ the lapse rate varied from 6.5 K km^{-1} at the poleward edge of the Hadley cell to 0 K km^{-1} at the ice/snow boundary (where H is the density scale height); beyond this boundary the lapse rate is kept at 0 K km^{-1}. Above $z = 0.25\ H$, the lapse rate is always taken to be 6.5 K km^{-1}. In the calculations we will present, the above lapse-rate adjustment is made over a layer between $z = 0$ and $z = 0.4\ H$. With the present IR flux calculations, this choice more accurately modeled the existing climate.[1]

The reader is referred to Lindzen and Farrell (1980) for a detailed description of this climate model. Our procedure is as follows: We take $F_\odot(T_*)$, as obtained in Section 3, to give the dependence of outgoing infrared flux on surface temperature. $F_\odot(T_*)$ is separately evaluated for four cases.

1) Present CO_2 and 6.5 K km^{-1} adjustment.
2) Present CO_2 and cumulus parameterization.
3) Double CO_2 and 6.5 K km^{-1} adjustment.
4) Double CO_2 and cumulus parameterization.

Coefficients for the polynomial fits to the calculated $F_\odot$ as a function of surface temperature, according to

$$F_\odot\,[\mathrm{W\ m^{-2}}] = \sum_{0}^{7} C'_i T_*^i\ [°\mathrm{C}],$$

are presented in Table 4. For solar flux and albedo we take the distributions given in Lindzen and Farrell as derived from Hartmann and Short (1979) models.[2]

In each case the Lindzen-Farrell Hadley-baroclinic adjustment yields a distribution of $\partial T_*(\theta)/\partial\theta$, where θ is the latitude. This distribution is inte-

[1] It was also necessary to reduce the outgoing longwave flux by ~11% to reproduce the present global mean temperature. This was necessary in order to compensate for the fact that our calculations of F slightly overestimate observed values (*viz.*, Fig. 11). We suspect that this discrepancy arises from the neglect of clouds in our IR calculations.

[2] The use of the Budyko-Sellers model instead does not significantly alter the present results. This may seem surprising in view of the contention in Lindzen and Farrell (1980) that the Budyko-Sellers parameters yield greater sensitivities. Such differences are obscured in the present case because doubling CO_2 moves the ice line to the poles for either choice. This arises because we are seeking a steady equilibrium response to annually-averaged solar forcing. The effect is not apparent in a time-dependent, seasonally-varying model integrated for relatively short periods such as 15 years (*viz.*, Manabe and Stouffer, 1980).

grated to obtain $T_*(\theta)$ within an integration constant. The integration constant is chosen so that

$$\int_0^{90°} F_\odot(T_*(\theta)) \cos\theta \, d\theta$$

equals the integral of incoming solar radiation. The procedure is iterated until a solution is obtained with the ice/snow line at the latitude where $T = -10°C$. Before proceeding to the results, we should note that our baroclinic adjustment assumes a static stability which generally is not the same as that for the profiles for which $F_\odot(T_*)$ is calculated. The differences are most noticeable for the "cumulus" parameterization in the tropics; however, in these regions baroclinic adjustments are negligible. Also, the temperature profiles resulting from our cumulus parameterization are far closer to observed profiles in the tropics (see Fig. 12). At high latitudes (and lower surface temperatures), the dependence of $F_\odot(T_*)$ on details of the vertical profile is very small. Thus, the discrepancy between the vertical profiles implicit in the calculation of $F_\odot(T_*)$ and in those assumed for baroclinic adjustment does not appear to have serious consequences.

Table 5 shows the global-mean temperature for each of our four cases. For comparison we also show the results from Section 3 obtained by averaging radiative-convective equilibria over all latitudes. We see that the cumulus parameterization again reduces model sensitivity to a doubling of CO_2 by $\sim$30%. Also the sensitivity in a global model with ice/snow feedbacks is $\sim$50% greater than in a globally-averaged radiative-convective equilibrium model. This is smaller than the increased sensitivity obtained by Manabe and Wetherald (1975), but later results by Manabe and Stouffer (1980) also show a reduced increase in sensitivity. Both Manabe and Wetherald (1975) and Manabe and Stouffer (1980) use general circulation models.

Fig. 14a shows the latitudinal distribution of surface temperature with the current concentration of

TABLE 5. Sensitivities of globally-averaged surface temperatures.

	6.5 K km^{-1} adjustment model			Cumulus model		
	Standard CO_2	Double CO_2	$\Delta\{T_*\}$	Standard CO_2	Double CO_2	$\Delta\{T_*\}$
$\{T_*\}$ (K) Climate model	289.38	292.15	2.77	287.87	289.80	1.93
$\{T_*\}$ (K) Radiative-convective equilibrium	276.45	278.37	1.92	275.86	277.13	1.27

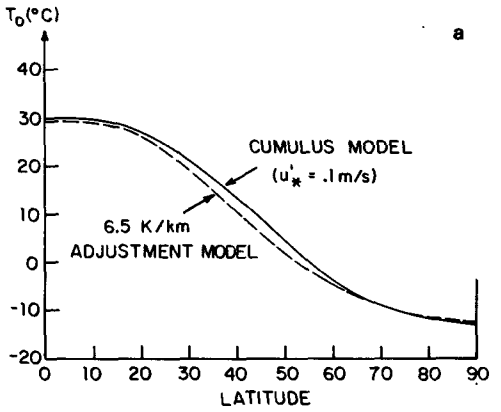

FIG. 14a. Surface temperature distributions calculated by the Hadley-baroclinic climate model for the standard CO_2 content using the radiative-convective adjustment model results.

CO_2 for the 6.5 K km^{-1} adjustment and parameterized cumulus models. The changes in T_0 resulting from doubling the CO_2 are given in Fig. 14b. Apart from the 30% reduction in sensitivity with cumulus parameterization there is little difference between the models. Temperature sensitivities in the tropics are somewhat smaller than globally-averaged sensitivities. On the other hand, at high latitudes sensitivities are about twice as large as the globally-averaged sensitivities. This striking latitudinal variation in sensitivity is again consistent with the general circulation model results of Manabe and Stouffer (1980), though Manabe and Stouffer get somewhat larger sensitivities at high latitudes.

The climate model results of the present section do not alter the conclusion of the previous section that the use of a physically-based convective parameterization modestly reduces sensitivity to doubling CO_2 relative to a model using convective adjustment. However, from Fig. 11 it is evident that if the present climate were much warmer the choice of convection model would also matter more.

Finally, this section shows the ease with which the Lindzen-Farrell model permits the extension of one-dimensional radiative-convective calculations to global calculations wherein ice/snow feedbacks can be included. However, certain results such as the virtual

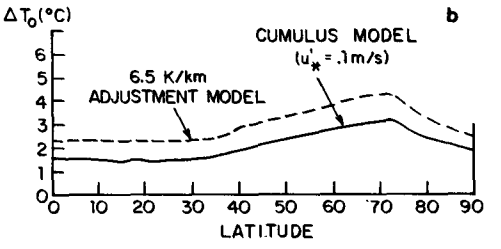

FIG. 14b. Surface temperature increases given by the Hadley-baroclinic climate model for doubled CO_2 content using the radiative-convective cumulus model results.

elimination of ice when CO_2 is doubled are likely to be unrealistic consequences of ignoring seasonal variations. The inclusion of an annual cycle is now being carried out.

5. Summary and conclusions

We have found that the effect of replacing the conventional 6.5 K km^{-1} lapse-rate adjustment with a physically-based, cumulus-type parameterization in a radiative-convective model is to reduce the model sensitivity to radiative perturbations significantly for tropical temperatures. No similar reduction in sensitivity is found at high latitudes. We have shown that these two convective models are qualitatively different at high surface temperatures. In regions where the surface temperature exceeds a value close to 288 K (comparable to the global mean), the 6.5 K km^{-1} adjustment model responds to increases in solar flux or CO_2 concentration by raising the surface temperature drastically without bound, but the cumulus model quickly reaches an equilibrium temperature in the neighborhood of 315 K. There are three reasons for this reduced sensitivity: 1) Heat lost from the surface through evaporation and upward sensible heat fluxes is deposited higher in the troposphere, where it is more effectively radiated to space; 2) the response in the convective heating is mostly confined to the cloud-top region, leading to a smaller greenhouse feedback through a reduced water vapor increase; and 3) with the additional degree of freedom allowed by a variable lapse rate, radiative perturbations near the tropopause can be accommodated locally, without being carried through a fixed lapse rate to the surface.

The implication of this result for global climate is assessed using the Lindzen-Farrell (1980) climate model. In terms of the global-mean surface temperature, the cumulus model is ~34% less sensitive compared to the 6.5 K km^{-1} adjustment model. The Lindzen-Farrell model also reproduces the following features found by Manabe and Wetherald (1975) and Manabe and Stouffer (1980) using a general circulation model: (i) ice/snow feedbacks amplify sensitivities by ~50% (globally-averaged temperature increases about 2°C for a doubling of CO_2); and (ii) climatic response is amplified at high latitudes. It should also be added that the Lindzen-Farrell model is only slightly more complicated than one-dimensional radiative-convective models. As such, it is a particularly useful tool for assessing climatic impacts.

Finally, it may be of interest to note that cumulus convection effectively inhibits any possibility of a runaway greenhouse on earth.

Acknowledgments. This work was supported by NASA Grant NGL-22-007-228 and by NSF Grant ATM-78-23330.

APPENDIX

The Radiative Model

We consider a simple non-grey radiative model with longwave absorptions by water vapor and carbon dioxide and shortwave ozone heating, assuming the contribution from shortwave absorption by water vapor is small (see Manabe and Strickler, 1964). For longwave radiative flux computations, we follow Rodgers' (1967) emissivity approximations. To calculate the heating rates due to ozone absorption of sunlight, we use Lindzen and Will's (1973) analytic formulation. Since the details and justifications of the various approximations for the radiative model are given in the references cited above, we will briefly summarize the model equations.

We solve for the state of radiative-convective equilibrium by forward time marching until a "steady state" is reached. This is usually taken to be when the heating rate is less than 10^{-5} K day^{-1} at all levels. The time rate of change of the air temperature is given by

$$\rho C_p \frac{dT}{dt} = Q_{H_2O} + Q_{CO_2} + Q_{O_3} + Q_c , \quad \text{(A1)}$$

where t is time, Q_c the convective heating rate discussed in Section 2, Q_{O_3} the ozone heating rate, and Q_{H_2O} and Q_{CO_2} are the long-wave heating rates due to water vapor and carbon dioxide, respectively, as given by

$$Q_a = -\frac{d(F_a^{\uparrow} - F_a^{\downarrow})}{dz} , \quad \text{(A2)}$$

where z is height, and $F_a^{\uparrow}$ and $F_a^{\downarrow}$ are the upward and downward long-wave radiative fluxes due to absorber a, respectively.

a. Longwave absorption by water vapor

In Eq. (6) of Rodgers (1967) the thermal emissivity ϵ for water vapor or carbon dioxide is given by a simple analytic expression in terms of the column density u, i.e.,

$$\left.\begin{aligned} \epsilon(u) &= \sum_1^N a_n u^{n/2}, \qquad u < v \\ &= \sum_0^N b_n (\ln u)^n, \qquad u > v \end{aligned}\right\} , \quad \text{(A3)}$$

where the coefficients a_n and b_n are numerical constants given in Rodgers' Table 2 (p. 52) for fitting upward or downward infrared fluxes, v is an adjustable parameter taken to be 10^{-3} g cm^{-2} for water vapor absorption, and u_{H_2O} (in units of g cm^{-2}) is the pressure-corrected amount of water vapor for the atmospheric path (z, z') measured from the level z to z'

$$u_{H_2O} = \int_z^{z'} q(\zeta)\rho(\zeta)\frac{p(\zeta)}{p_*}\,d\zeta, \qquad (A4)$$

where q is the mass mixing ratio of water vapor defined in (3b), ρ the air density, p the pressure of the environment, and p_* a reference surface pressure taken to be 1000 mb. When (A3) is employed for downward flux calculations, $z' \geq z$, but when computing upward fluxes $z' \leq z$, so that $u_{H_2O}(z, z')$ is non-negative and $u_{H_2O}(z, z) = 0$.

The downward radiative flux $F^{\downarrow}_{H_2O}$ can be expressed as

$$F^{\downarrow}_{H_2O}(z) = \int_0^{U_{H_2O}} B(u_{H_2O})\frac{d\epsilon_{H_2O}}{du_{H_2O}}\,du_{H_2O}, \qquad (A5)$$

where U_{H_2O} is the total amount of u_{H_2O} above the level z, $B(u) = \sigma T^4(u)$, and σ is the Stefan-Boltzmann constant. The upward flux $F^{\uparrow}_{H_2O}$ is given by

$$F^{\uparrow}_{H_2O}(z) = \sigma T_*^4 + \int_0^{U_{H_2O}} [B(u_{H_2O}) - B(U_{H_2O})] \times \frac{d\epsilon_{H_2O}}{du_{H_2O}}\,du_{H_2O}, \qquad (A6)$$

where u_{H_2O} is here measured downward from z, and for the flux condition at the lower boundary it is assumed that the ground radiates as a blackbody at temperature T_*, and the upward infrared flux at the surface is given by σT_*^4. As mentioned in Section 2, in the conventional 6.5 K km^{-1} lapse-rate adjustment model T_* is given by $T(0)$, the air temperature at $z = 0$, and the radiative flux balance at the surface determines the integrated convective heating Q_c, which in turn sets a constraint on the total heat flux that can be carried upward through the adjustment of lapse rates. In cases of parameterized surface energy fluxes, a temperature discontinuity is allowed at the ground by requiring T_* to satisfy the condition

$$\sigma T_*^4 = F^{\downarrow}_{H_2O}(0) + F^{\downarrow}_{CO_2}(0) + F_{\odot *} - (LE + F_s), \qquad (A7)$$

where $F_{\odot *}$ is the solar flux absorbed at the ground, and E and F_s are given by (2a) and (2b) as functions of T_*, $T(0)$, and the surface drag parameter $C_D u_*$.

b. Longwave absorption by carbon dioxide

Carbon dioxide radiation is assumed to be contained in a 200 cm^{-1} interval centered ~667 cm^{-1}. The formulation given by Rodgers (1967) allows the overlap of H_2O by means of a statistical model fitted to the same region. The emissivity of CO_2 is given in the same form as (A3) with the a_n and b_n coefficients for CO_2 taken from Table 2 of Rodgers and $v = 0.01$ cm-atm. The volume mixing ratio of CO_2 is taken to be 3.2×10^{-4}. To obtain the column density u_{CO_2} in units of cm atm^{-1} for the emissivity formula, we compute the column number density n_{CO_2} by

$$n_{CO_2}(\text{cm-atm cm}^{-1}) = \frac{\rho_{CO_2}}{\rho_{CO_2/STP}} = 3.32 \times 10^{-2}\left(\frac{p}{p_*}\right),$$

which gives

$$u_{CO_2}(z, z') = \int_z^{z'} n_{CO_2}\left(\frac{p}{p_*}\right)d\zeta. \qquad (A8)$$

As before, the path of integration is measured from the level z, with $z' \geq z$ for downward fluxes and $z' \leq z$ for upward fluxes.

The infrared flux contributions due to CO_2 are

$$F^{\downarrow}_{CO_2}(z) = 200\int_z^{\infty} B_{667}(z')\frac{d}{dz'} \times [\epsilon_{CO_2}(z, z')\tilde{T}_{H_2O}(z, z')]dz', \qquad (A9)$$

$$F^{\uparrow}_{CO_2}(z) = 200\left\{\int_z^0 B_{667}(z')\frac{d}{dz'} \times [\epsilon_{CO_2}(z, z')\tilde{T}_{H_2O}(z, z')]dz' - B_{667}(0)\epsilon_{CO_2}(z, 0)\tilde{T}_{H_2O}(z, 0)\right\}, \qquad (A10)$$

where $B_{667}(z')$ is the Planck function (in terms of flux rather than intensity) centered at 667 cm^{-1}; $\tilde{T}_{H_2O}(z, z')$ is the water vapor transmission between levels z and z' according to Goody's (1964) statistical model. The statistical model constants are $k/\delta = 7.345$, $k/\pi\alpha_0 = 142.47$, $a = 1.66 \times 10^{-2}$, $b = -4.94 \times 10^{-5}$, $a' = 1.76 \times 10^{-2}$ and $b' = 5.66 \times 10^{-5}$ [as given in Rodgers and Walshaw (1966)].

c. Shortwave heating by ozone

We consider ozone absorptions in the Hartley (2000–3000 Å), Huggins (>3000 Å) and Chappuis (5000–7000 Å) bands. Radiative heating due to these bands to a high degree of approximation can be modelled by an analytical formula given by Lindzen and Will (1973), *viz.*,

$$\frac{Q_{O_3}}{n_{O_3}} = I_H K_H \Delta\lambda_H \exp(-K_H u_{O_3}) + I_C K_C \Delta\lambda_C \exp(-K_C u_{O_3}) + \frac{I_{Hu}}{m u_{O_3}}\{\exp[-K_{Hu}u_{O_3}\exp(-m\lambda_{long})] - \exp[-K_{Hu}u_{O_3}\exp(-m\lambda_{short})]\}, \qquad (A11)$$

where Q_{O_3} is the heating rate [ergs s^{-1} cm^{-3}], n_{O_3} the

ozone density [cm NTP cm^{-1}], I the mean intensity of a particular band, K the absorption coefficient, λ the wavelength (Å), $\Delta\lambda$ an averaged wavelength interval, m is a numerical constant, subscripts H, C and Hu denote Hartley, Chappuis and Huggins bands, respectively; and u_{O_3} is the column density of ozone given by

$$u_{O_3}(\text{cm NTP}) = \int_z^\infty n_{O_3} dz'/\cos\psi, \quad \text{(A12)}$$

where z is height and ψ the zenith angle. For the best fit to within 5% of Craig's calculation of Q_{O_3}/n_{O_3}, the following parametric values are given by Lindzen and Will (1973):

For Hartley bands

$$I_H = 9 \text{ ergs cm}^{-2} \text{ s}^{-1} \text{ Å}^{-1}$$

$$K_H = 260 \text{ cm NTP}^{-1}$$

$$\Delta\lambda_H = 375 \text{ Å}.$$

For Chappuis bands

$$I_C = 180 \text{ ergs cm}^{-2} \text{ s}^{-1} \text{ Å}^{-1}$$

$$K_C = 0.118 \text{ cm NTP}^{-1}$$

$$\Delta\lambda_C = 1650 \text{ Å}.$$

For Huggins bands

$$K_{Hu} = 1.99 \times 10^{17} \text{ cm NTP}^{-1}$$

$$m = 0.0126$$

$$I_{Hu} = 53 \text{ ergs cm}^{-2} \text{ s}^{-1} \text{ Å}^{-1}$$

$$\lambda_{short} = 2750 \text{ Å}$$

$$\lambda_{long} = 3400 \text{ Å}.$$

The ozone data are taken from Herring and Borden (1965, 1967) and Prather (1981). For typical midlatitude values, we have used the seasonal data for 30°N. The heating rates are calculated for seasonally-averaged zenith angles and ozone amounts, from which we obtain the annual-mean heating rates as a function of height.

REFERENCES

Bacastow, R., and C. D. Keeling, 1973: *Carbon and the Biosphere*, G. M. Woodwell and E. V. Pecan, Eds. USAEC CONF-720510, U.S. Atomic Energy Commission, Springfield, VA, 86–135.

Chylek, P., and J. T. Kiehl, 1981: Sensitivities of radiative convective climate models. *J. Atmos. Sci.*, **38,** 1105–1110.

Goody, R. M., 1964: *Atmospheric Radiation.* Oxford University Press, 436 pp.

Hansen, J., D. Johnson, A. Lacis, S. Lebedeff, P. Lee, D. Rind and G. Russell, 1981: Climate impact of increasing atmospheric carbon dioxide. *Science,* **213,** 957–966.

Hartmann, D. L., and D. A. Short, 1979: On the role of zonal asymmetries in climate change. *J. Atmos. Sci.*, **36,** 519–528.

Held, I. M., and M. J. Suarez, 1974: Simple albedo feedback models of the icecaps. *Tellus,* **26,** 613–629.

Herring, W. S., and T. R. Borden, Jr., 1965: Mean distributions of ozone density over North America, 1963–1964. Environ. Res. Pap. No. 162, AFCRL-65-913, Air Force Cambridge Research Lab., 19 pp.

——, and ——, 1967: Ozonesonde observations over North America. Environ. Res. Pap., No. 279, AFCRL-64-30, Vol. 4, Air Force Cambridge Research Lab.

Hoffert, M. I., 1974: Global distributions of atmospheric carbon dioxide in the fossil-fuel era: A projection. *Atmos. Environ.,* **8,** 1225–1249.

Hummel, J. R., and W. R. Kuhn, 1981a: Comparison of radiative-convective models with constant and pressure-dependent lapse rates. *Tellus,* **33,** 254–261.

——, and ——, 1981b: An atmospheric radiative-convective model with interactive water vapor transport and cloud development. *Tellus,* **33,** 372–381.

Ingersoll, A. P., 1969: The runaway greenhouse: A history of water on Venus. *J. Atmos. Sci.*, **26,** 1191–1198.

Keeling, C. D., R. B. Bacastow, A. E. Bainbridge, C. A. Ekdahl, P. R. Guenther, L. S. Waterman and H. F. S. Chin, 1976: Atmospheric carbon dioxide variations at Mauna Loa Observatory, Hawaii. *Tellus,* **28,** 538–551.

Lindzen, R. S., 1978: Some aspects of convection in Meteorology. *Problems of Stellar Convection,* E. A. Spiegel and J. Zahn, Eds., *Lect. Notes Phys.*, **71,** 128–141.

——, 1979: *Proc. Seminar on the Impact of Gate on Large-Scale Numerical Modeling of the Atmosphere and Ocean.* The National Research Council, Woods Hole, MA, 276 pp.

——, 1981: Some remarks on cumulus parameterization. *Clouds in Climate: Modeling and Satellite Observational Studies,* Rep. of Workshop held at NASA Goddard Institute for Space Studies, 222 pp.

——, and D. I. Will, 1973: An analytic formula for heating due to ozone absorption. *J. Atmos. Sci.*, **30,** 513–515.

——, and B. Farrell, 1980: The role of polar regions in global climate, and a new parameterization of global heat transport. *Mon. Wea. Rev.*, **108,** 2064–2079.

Manabe, S., 1971: Estimate of future changes of climate due to man's increase of carbon dioxide concentration in the air. *Man's Impact on Climate,* W. H. Mattews, W. W. Kellogg and G. D. Robinson, Eds., The MIT Press, 594 pp.

——, and R. F. Strickler, 1964: Thermal equilibrium of the atmosphere with a convective adjustment. *J. Atmos. Sci.*, **21,** 361–385.

——, and R. T. Wetherald, 1967: Thermal equilibrium of the atmosphere with a given distribution of relative humidity. *J. Atmos. Sci.*, **24,** 241–259.

——, and ——, 1975: The effects of doubling the CO_2 concentration on the climate of a general circulation model. *J. Atmos. Sci.*, **32,** 3–15.

——, and R. J. Stouffer, 1979: A CO_2-climate sensitivity study with a mathematical model of the global climate. *Nature,* **282,** 491–493.

——, and ——, 1980: Sensitivity of a global climate model to an increase of CO_2 concentration in the atmosphere. *J. Geophys. Res.*, **85,** 5529–5554.

——, and R. T. Wetherald, 1980: On the distribution of climate change resulting from an increase in CO_2 content of the atmosphere. *J. Atmos. Sci.*, **37,** 99–118.

Minzner, R. A., 1977: The 1976 standard atmosphere and its relationship to earlier standards. *Rev. Geophys. Space Phys.*, **15,** 375–384.

Oort, A. H., and E. M. Rasmusson, 1971: *Atmospheric Circulation Statistics.* NOAA Prof. Pap. No. 5, 323 pp.

Prather, M., 1981: Ozone in the upper stratosphere and mesosphere. *J. Geophys. Res.*, **86,** 5325–5338.

Priestly, C. H. B., 1959: *Turbulent Transfer in the Lower Atmosphere.* The University of Chicago Press, 130 pp.

Ramanathan, V., 1981: The role of ocean-atmosphere interactions in the CO_2 climate problem. *J. Atmos. Sci.*, **38,** 918–930.

——, and J. A. Coakley, 1978: Climate modeling through radiative-convective models. *Rev. Geophys. Space Phys.*, **16,** 465–489.

——, M. S. Lian and R. D. Cess, 1979: Increased atmospheric CO_2: Zonal and seasonal estimates of the effect on the radiation energy balance and surface temperature. *J. Geophys. Res.*, **84,** 4949–4958.

Raschke, E., T. H. Vonder Haar, R. W. Bandeen and M. Pasternak, 1973: The annual radiation balance of the earth atmosphere system during 1969–1970 from Nimbus 3 measurements. *J. Atmos. Sci.*, **30,** 341–364.

Rasool, S. I., and G. DeBergh, 1970: The runaway greenhouse and the accumulation of CO_2 in the Venus atmosphere. *Nature,* **226,** 1037–1039.

Rodgers, C. D., 1967: The use of emissivity in atmospheric radiation calculations. *Quart. J. Roy. Meteor. Soc.*, **93,** 43–54.

Rodgers, C. D., and C. D. Walshaw, 1966: The computation of infrared cooling rate in planetary atmospheres. *Quart. J. Roy. Meteor. Soc.*, **92,** 67–92.

Sarachik, E. S., 1978: Tropical sea surface temperature: An interactive one-dimensional atmosphere-ocean model. *Dyn. Atmos. Oceans,* **2,** 455–469.

Schneider, E. K., 1977: Axially symmetric steady-state models of the basic state for instability and climate studies. Part II: Nonlinear calculations. *J. Atmos. Sci.*, **34,** 280–297.

Schneider, S. H., 1975: On the carbon dioxide-climate confusion. *J. Atmos. Sci.*, **32,** 2060–2066.

Stevens, D., and R. S. Lindzen, 1978: Tropical wave-CISK with a moisture budget and cumulus friction. *J. Atmos. Sci.*, **35,** 940–961.